International Refereed Journal of Engineering and Science (IRJES)
ISSN (Online) 2319-183X, (Print) 2319-1821
Volume 1, Issue 2 (October 2012), PP.01-10
www.irjes.com

Assessment Of Relative Atmospheric Normalization For Multi-Temporal Worldview-2 Data

Mohamed Elhabiby [1,3] ,Ahmed Elsharkawy [1,2] & Naser El-Sheimy [1,4]
[1]*Dept. of Geomatics Engineering, University of Calgary, Calgary, Alberta, T2N 1N4*
Phone: 403-210-7897, Fax: 403-284-1980,
[3]*Public Works Department, Faculty of Engineering, Ain Shams University, Cairo, Egypt.*

ABSTRACT : *WorldView-2 products delivered to the customer are radiometrically corrected image pixels. The values of these pixels are calculated as a function of the amount of spectral radiance that enters the telescope aperture which is then converted into corresponding digital values. Consequently, image pixel data are unique to WorldView-2 and should not be directly compared to imagery from other sensors of a radiometric/spectral prospective. Instead, image pixels should be converted to top-of-atmosphere spectral radiance. However, this top-of-atmosphere spectral radiance varies with Earth-Sun distance, solar zenith angle, topography, and atmospheric effects (absorption and scattering). To account for these variations, top-of-atmosphere spectral radiance should be converted into reflectance so it can be used in spectral analysis techniques such as band ratios, Normalized Difference Vegetation Index (NDVI), matrix transformations, etc.*
In order to ensure the reliability of multi-temporal data, a further radiometric normalization step is required and should include relative or absolute atmospheric correction for each image in the time series. The challenge, however, with absolute radiometric calibration is the difficulty in obtaining an atmospheric characterization at a given acquisition date since it requires knowledge of the atmospheric properties at the time of acquisition— a difficult task even when planned, and of course for most historic satellite data[1]. In this paper, we investigate the quality of the relative atmospheric calibration step through a process of radiometric calibration beginning with a conversion to radiance then to reflectance and finally with the application of relative atmospheric correction. Six scenes covering a wide variety of features from well-structured urban areas to desert areas and shallow lakes to deep ocean water will be used. These scenes are from Brisbane, Miami, Rio de Janeiro, Cairo, San Francisco and Ismailia and were provided by DigitalGlobe. They include different dates, sun angle elevation, earth-sun distances and various angles of acquisition. The sixth scene for Ismailia was considered the master scene. The process first involved a transformation to the top of atmosphere reflectance for the six dates, followed by the application of a relative atmospheric calibration using Pseudo Invariant Features that were manually selected for the five classes to account for the atmospheric attenuation. Finally, a multi-layer classification algorithm was applied to the master and slave scenes after atmospheric normalization. The classification results were compared and used as a quality control measure for the radiometric calibration parameters provided by the given Metadata file from the data service provider. When the multi-layer classification algorithm was applied to the six scenes without changing the thresholds, the classification results show very good potentials for the use of a relative atmospheric calibration step when dealing with multi-temporal data. Conclusions and recommendations are then given with respect to the transferability, accuracy and efficiency of the thresholds and to the calibration process.

Keywords*: Radiometric calibration, Relative atmospheric calibration, Multi-layer classification, High resolution satellite imagery, Multi-temporal data.*

I. INTRODUCTION

Multi-temporal high resolution satellite imagery is one of the most important tools for urban planning, change detection and trend analysis[2].In order to obtain accurate quantitative information from multispectral satellite data, such as WorldView-2, a conversion of raw digital numbers (DN) to reflectance values is required. Since a uniform scene does not create a uniform image in terms of raw DN relative radiometric calibration and correction are necessary. Major causes of non-uniformity include variability in detector response, variability in electronic gain and offset, lens falloff and particulate contamination on the focal plane[3]. The apparent effects of this non-uniformity on the final product will be in the form of:

- Random bad pixels
- Line start/end problems
- Full or partial line-column drop-outs
- Line or column striping

Normally, WorldView-2 products are delivered free of the aforementioned deficiencies. However, to ensure a reliable use of multi-temporal data from the same or different satellite, a further radiometric normalization step is required. This step should account for earth-sun distance, azimuth angle, and relative/absolute atmospheric correction for each image in the time series. The main problem here is the difficulty in obtaining an atmospheric characterization at a given acquisition date since it requires knowledge of the atmospheric properties at the time of acquisition which is a difficult task even when planned and of course for most historic satellite data[1]. In this paper, we investigate the quality of the relative atmospheric calibration step through a process of radiometric calibration beginning with a conversion to radiance then to reflectance and finally with the application of a relative atmospheric correction. Six scenes covering a wide variety of features ranging from well-structured urban areas to desert areas and shallow lakes to deep ocean water will be used. These scenes are from Brisbane, Miami, Rio de Janeiro, Cairo, San Francisco and Ismailia, and were provided by the DigitalGlobe. They include different dates, sun angle elevation, earth-sun distances and different angles of acquisition. The sixth scene for Ismailia was considered the master scene. The process first involved a transformation to the top of atmosphere reflectance for the six dates, followed by the application of a relative atmospheric calibration using Pseudo Invariant Features that were manually selected for five classes to account for the atmospheric attenuation. Finally, a multi-layer classification algorithm was applied to the master and slave scenes after atmospheric normalization. The classification results were compared and used as a quality control measure for the radiometric calibration parameters provide by the given Metadata file from the data service provider.

II. DATA AND METHOD

WorldView-2 is the first commercial high-resolution satellite to provide eight spectral sensors in the visible to near-infrared range. Each sensor is closely focused on a particular range of the electromagnetic spectrum, which is sensitive to a specific feature on the ground. Together, they are designed to improve the segmentation and classification of land and marine features[4]. Figure 1 is a brief comparison of spectral and panchromatic bands from QuickBird, GeoEye-1, IKONOS and WorldView-2.

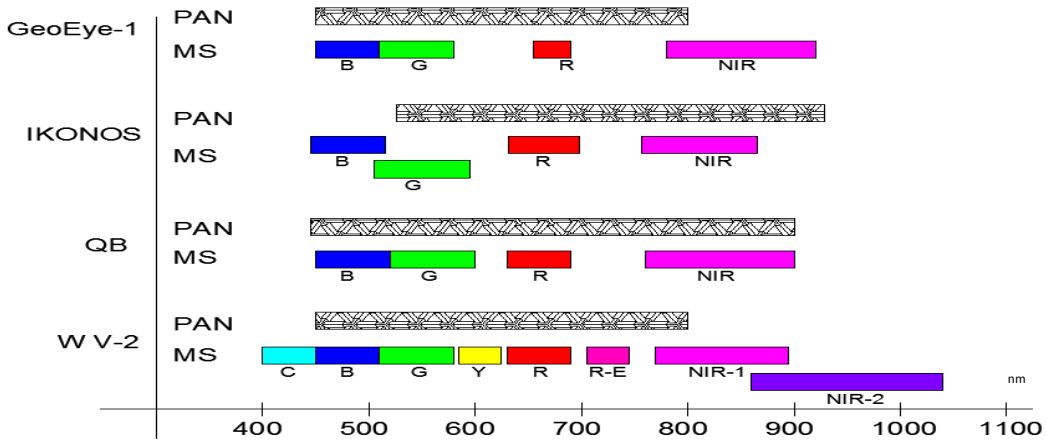

Figure 1 Panchromatic and multispectral wavelengths for different satellites,[5]

In general, the new spectral bands of WorldView-2 (Coastal blue, Yellow, Red edge and NIR-2) target coastal and vegetation land cover types with applications in plant species identification, vegetation stress and crop type mapping, wetlands and coast water quality, and bathymetry [6] . More specifically, the Yellow and Red edge bands fill important gaps in the spectrum as related to the ability of capturing vegetation [7]. Moreover, Coastal blue and NIR2 bands are very helpful distinguishing different types of vegetation and many man-made objects [8].

1.1 Area of study

The following table summarizes the details of the areas of study

Table 1. Data description of the selected areas of study

Area	Date of acquisition	Time of acquisition	Mean Sun elevation angle	Mean off-Nadir Angle	Coordinates	
					NW corner	SE corner
Brisbane, Australia	2011-07-13	12:19 PM	35.8	4.2	Lat = -27.39834702; Long = 152.92576820;	Lat = -27.58007339; Long = 153.09455130;
San Francisco USA	2011-10-09	07:36 PM	45.8	19.6	Lat = -37.81769; Long = -122.52874;	Lat = 37.6884861; Long = -122.347665
Miami, USA	2010-11-12	04:08 PM	44.5	21.8	Lat = 25.79358766; Long = -80.23388183;	Lat = 25.77095011; Long = -80.19061897
Rio De Janeiro, Brazil	2011-01-25	01:11 PM	63.3	21.6	Lat = -22.63268039; Long = -43.34973594;	Lat = -22.98754875; Long = -43.15856103;
Cairo, Egypt	2010-01-15	08:41 AM	35.3	18	Lat = 30.10896873; Long = 31.18571091;	Lat = 29.98427391; Long = 31.29685211;
Ismailia, Egypt	2011-04-16	08:42 AM	64.2	27.6	Lat = 30.63333000; Long = 32.14056000;	Lat = 30.53750000; Long = 32.33333000;

The data was provided in tiles, rows and columns, and we tried to choose the mid row-col. scene of each area. Figure 2 illustrate a false color composite, NIR-1 G B, of the selected study areas.

Brisbane, Australia

Cairo, Egypt

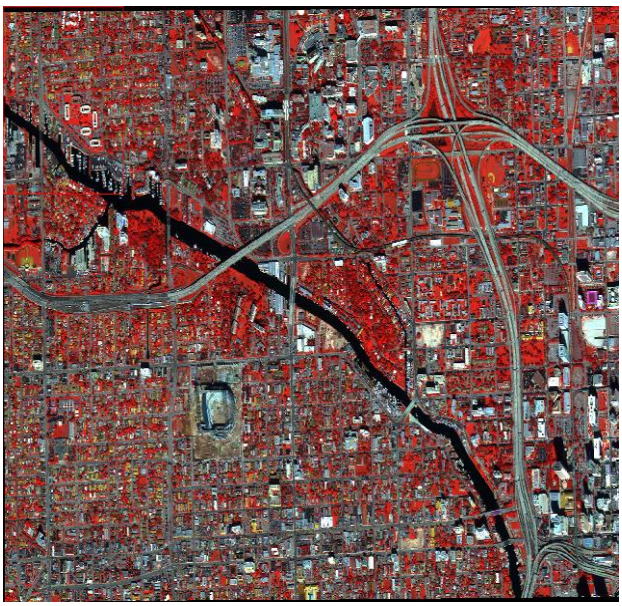

Miami, USA

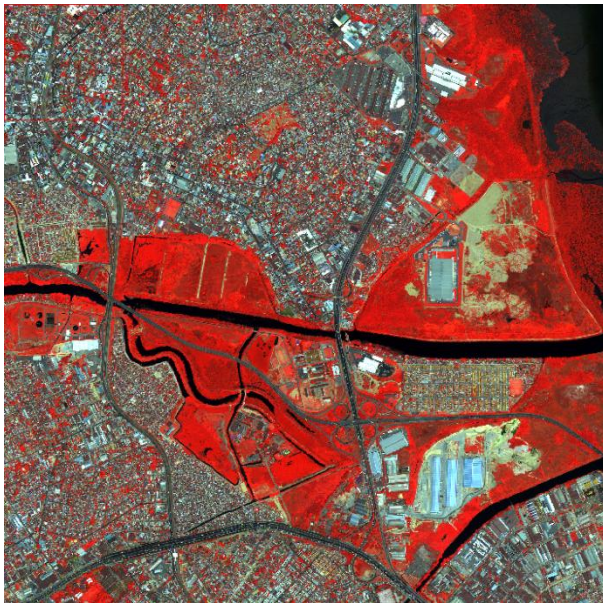

Rio De Janeiro, Brazil

Ismailia, Egypt

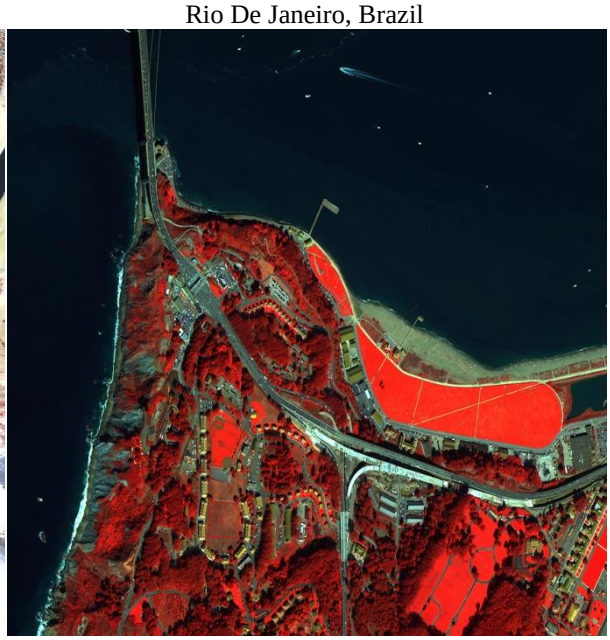

San Francisco

Figure 2 Area of study

1.2 Methodology

Generally, any imagery used in radiometric/spectral analysis must be converted to spectral radiance at a minimum or top of atmosphere reflectance in order to account for the variation in relative positions between the sun, the earth and the satellite and to obtain an absolute value for the NDVI ratios which can be applied to any other scene [3]. Converting the Digital Numbers (DN) to top of atmosphere (ToA) reflectance is a two-step process. First the DNs are converted to ToA radiance values. Then, these radiance values are converted to reflectance values[9].

Conversion to Top-of-Atmosphere Spectral Radiance. According to [10], WorldView-2 products are delivered to the customer as radiometrically corrected image pixels. The values of these pixels are calculated as a function of the amount of spectral radiance that enters the telescope aperture and the instrument conversion of that radiation into a digital signal. Therefore, image pixel data are unique to WorldView-2 and should not be directly compared to imagery from other sensors, radiometrically or spectrally speaking. Instead, image pixels should be at least converted to top of atmosphere spectral radiance. Top of atmosphere spectral radiance is defined as the spectral radiance entering the telescope aperture at the WorldView-2 altitude of 770 km. The conversion from

radiometrically corrected image pixels to spectral radiance uses the following general equation for each band of a WorldView-2 product[3]:

$$L_{\lambda_{pixel,band}} = \frac{K_{band} \cdot q_{pixel,band}}{\Delta\lambda_{band}} \qquad \text{Eq. 1}$$

Where, $L_{\lambda_{pixel,band}}$ are the top of atmosphere spectral radiance image pixels [W.m-2.sr-1.µm-1],
K_{band} is the absolute radiometric calibration factor [W.m-2.sr-1.count-1] for a given band,
$q_{pixel,band}$ are the given radiometrically corrected image pixels [counts] and
$\Delta\lambda_{band}$ is the effective bandwidth [μm] for a given band

Both K_{band} and $\Delta\lambda_{band}$ can be found in the image Metadata files (*.IDM) attached with the WorldView-2 product under the names absCalFactor and effectiveBandwidth, respectively. The following table summarizes both of these quantities for the panchromatic and the 8 multi-spectral bands.

Table 1. Absolute radiometric calibration and effective bandwidth for the given bands

Band name	K_{band} W.m^{-2}.sr^{-1}.count^{-1}	$\Delta\lambda_{band}$ μm
C	9.30E-03	4.73E-02
B	1.78E-02	5.43E-02
G	1.36E-02	6.30E-02
Y	6.81E-03	3.74E-02
R	1.10E-02	5.74E-02
R-E	6.06E-03	3.93E-02
NIR1	1.22E-02	9.89E-02
NIR2	9.04E-03	9.96E-02

Conversion to top of-atmosphere spectral reflectance: Currently we have the ToA spectral radiance. However, this top of atmosphere spectral radiance varies with Earth-Sun distance, solar zenith angle, topography, bi-directional reflectance distribution function (BRDF-the target reflectance varies depending on the illumination and observation geometry), and atmospheric effects (absorption and scattering)[3]. As previously mentioned, it is imperative that multispectral data be converted into reflectance prior to performing spectral analysis techniques such as band ratios, Normalized Difference Vegetation Index (NDVI), matrix transformations, etc.. There are several factors that must be known for each scene: the distance between the sun and earth in astronomical units, the day of the year (Julian date), and solar zenith angle.

$$JD = int[356.25.(year + 4716)] + int[30.6001.(month + 1)] + day + \frac{UT}{24} + B - 1524.5 \qquad \text{Eq. 2}$$

$$d_{ES}=1.00014-0.01671.\cos(g)-0.00014.\cos(2g) \qquad \text{Eq. 3}$$

The Earth-Sun distance will be in Astronomical Units (AU) and should have a value between 0.983 and 1.017. For the WorldView-2 launch date, October 8, 2009 at 18:51:00 GMT corresponding to the Julian Day 2455113.285; the Earth-Sun distance is 0.998987 AU. At least six decimal places should be carried in the Earth-Sun distance for use in radiometric balancing or top of atmosphere reflectance calculations[3].
The average solar Zenith angle must be calculated for the whole scene at the time of acquisition according to the following equation:

$$\theta_s = 90.0 - sunEL \qquad \text{Eq. 4}$$

Where the *sunEl* value can be found in the same file *.IDM. Now we can convert the radiance values to ToA reflectance values using the following equation:

$$\rho_{\lambda_{pixel\ ,band}} = \frac{L_{\lambda_{pixel\ ,band}} .{d_{ES}}^2 .\pi}{E_{sun\ \lambda_{band}} .\cos(\theta_s)} \qquad \text{Eq. 5}$$

Where $\rho_{\lambda_{pixel\ ,band}}$ are the ToA reflectance values
$L_{\lambda_{pixel\ ,band}}$ are the ToA radiance values
d_{ES} is the Earth-Sun distance in Astronomical Units (AU)
$E_{sun\ \lambda_{band}}$ WorldView-2 Band-Averaged Solar Spectral Irradiance [3]
θ_s The average solar Zenith angle

Relative atmospheric calibration: The next step involves relative calibration of the atmospheric effect by normalizing the reflectance values of the slave scenes to the master scene using regression line. Ten points for each class were chosen as PIF's points throughout the five scenes covering the entire reflectance values and have the following properties:

- be spectrally homogenous; near lambertian and flat surfaces;
- minimal amount of vegetation;
- cover an area greater than three times the pixel size of the sensor;
- and, most importantly, exhibit minimum change in spectral characteristics over time.

Good examples of PIF's are: open water points, concrete slabs, sport field grass, bare soil. Table 2 demonstrates the average reflectance values of the chosen PIF's for each class in the six scenes and through the eight bands.

Table 2. PIF's average reflectance values in the six scenes for the eight bands

	C						B					
	Ismailia	Cairo	Brisbane	Miami	Rio de Janero	San Francisco	Ismailia	Cairo	Brisbane	Miami	Rio de Janero	San Francisco
Vegetation	0.1778	0.2586	0.1490	0.1841	0.1547	0.1745	0.1714	0.1484	0.1200	0.1551	0.1276	0.1397
Water	0.1752	0.2571	0.1494	0.1720	0.1495	0.1782	0.1664	0.1473	0.1290	0.1334	0.1149	0.1446
Asphalt	0.1919	0.2719	0.1801	0.2729	0.1886	0.2269	0.1902	0.1602	0.1667	0.2935	0.1727	0.2097
Building	0.2321	0.2876	0.1901	0.3155	0.2492	0.3599	0.2533	0.1763	0.1829	0.3412	0.2591	0.3892
Shadow	0.1797	0.2548	0.1471	0.18065		0.1739	0.1683	0.1461	0.1158	0.1410		0.1325
	G						Y					
Vegetation	0.1665	0.1392	0.1032	0.1456	0.1232	0.1179	0.1591	0.2233	0.0828	0.1184	0.0930	0.0857
Water	0.1543	0.1352	0.1063	0.0892	0.07465	0.1050	0.1483	0.2156	0.0879	0.0649	0.05242	0.0685
Asphalt	0.1767	0.1515	0.1446	0.2819	0.1493	0.1791	0.176	0.2511	0.1343	0.2664	0.1457	0.1596
Building	0.2662	0.1769	0.1718	0.3275	0.2575	0.3784	0.2869	0.3049	0.1595	0.3047	0.26429	0.3619
Shadow	0.1489	0.1331	0.0795	0.09266		0.08582	0.1475	0.2147	0.0612	0.0693		0.0593
	R						R-E					
Vegetation	0.1558	0.1586	0.06784	0.1014	0.0725	0.06694	0.2507	0.2691	0.2187	0.2618	0.2557	0.2267
Water	0.1427	0.1526	0.0757	0.05239	0.0439	0.0536	0.1413	0.2050	0.0513	0.0404	0.0372	0.0344
Asphalt	0.1811	0.1838	0.1331	0.2819	0.1423	0.1615	0.18694	0.25675	0.1396	0.2568	0.1391	0.1507
Building	0.3024	0.2257	0.1568	0.3227	0.2657	0.3816	0.3075	0.3170	0.1543	0.2914	0.25572	0.3476
Shadow	0.1455	0.1519	0.0519	0.0562		0.0467	0.14892	0.2138	0.0533	0.0545		0.0529
	NIR-1						NIR-2					
Vegetation	0.3572	0.2314	0.3991	0.4068	0.4511	0.4187	0.3032	0.2757	0.3563	0.3327	0.3490	0.3504
Water	0.1416	0.1475	0.0395	0.0349	0.0393	0.0250	0.1104	0.1675	0.0292	0.0281	0.0274	0.0170
Asphalt	0.2045	0.1919	0.1499	0.2840	0.1482	0.1604	0.1689	0.22607	0.1295	0.2151	0.1166	0.1269
Building	0.3292	0.2381	0.1702	0.3144	0.2803	0.3613	0.2701	0.2775	0.1530	0.2521	0.2093	0.2906
Shadow	0.1556	0.1571	0.0559	0.0505		0.0591	0.1275	0.1817	0.0481	0.0410		0.0473

A summary of the algorithm is in Figure 3.

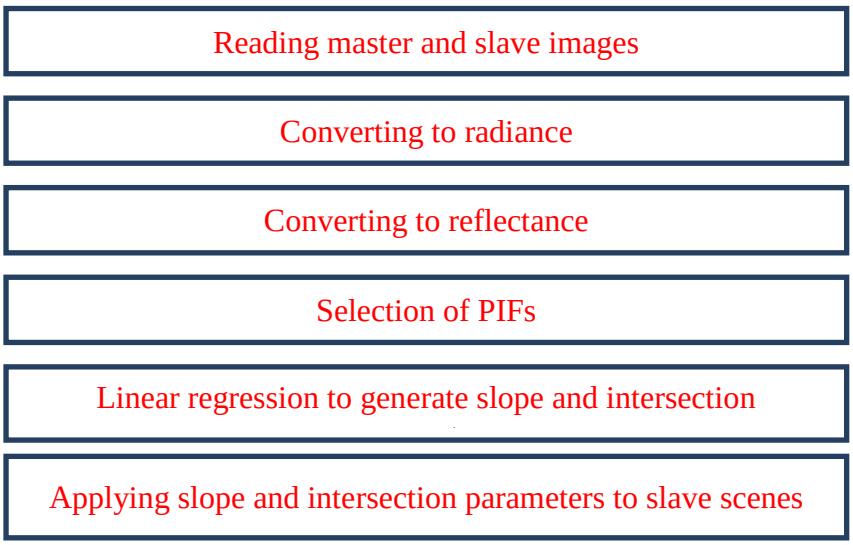

Figure 3 summary of the calibration algorithm

The linear least square regression is a procedure in which the coefficients a_1 and a_0 of a linear function $y=a_1x+a_o$ are determined, such that the function has the best fit to a given set of data points[11]. For a given set of n data points (x_i, y_i) the solution of this system is:

$$a_1 = \frac{n\sum_{i=1}^{n} x_i y_i - (\sum_{i=1}^{n} x_i)(\sum_{i=1}^{n} y_i)}{n\sum_{i=1}^{n} x_i^2 - (\sum_{i=1}^{n} x_i)^2} \qquad \text{Eq. 6}$$

$$a_o = \frac{(\sum_{i=1}^{n} x_i^2)(\sum_{i=1}^{n} y_i) - (\sum_{i=1}^{n} x_i y_i)(\sum_{i=1}^{n} x_i)}{n\sum_{i=1}^{n} x_i^2 - (\sum_{i=1}^{n} x_i)^2} \qquad \text{Eq.7}$$

$$E = R^2 = \sum_{i=1}^{n} [y_i - (a_1 x_i + a_o)]^2 \qquad \text{Eq.8}$$

Linear regression against the Ismailia scene was done for each band. And the next table illustrates the five regression lines with their confidence level R^2.

Table 3 regression line parameters for the 5 slave scenes

Band	C			B			G			Y		
Value	Intercept. a_o	Slope a_1	R^2	Intercept. a_o	Slope a_1	R^2	Intercept. a_o	Slope a_1	R^2	Intercept. a_o	Slope a_1	R^2
Cairo	-0.119	1.1598	0.836	-0.0182	1.3314	0.868	-0.128	2.0849	0.9227	-0.12	1.2367	0.9474
Brisbane	0.1744	0.1026	0.3666	0.172	0.1177	0.383	0.1618	0.1529	0.4416	0.1598	0.1983	0.512
Miami	0.1436	0.2076	0.702	0.145	0.2054	0.6279	0.1354	0.2488	0.6618	0.1308	0.3178	0.7416
Rio de janero	0.155	0.2027	0.4913	0.1552	0.224	0.5097	0.1482	0.2615	0.6001	0.1434	0.3176	0.71
San Francisco	0.1223	0.24	0.9708	0.1248	0.3257	0.9595	0.1229	0.3431	0.9348	0.1288	0.3615	0.8854
Band	R			R-E			NIR-1			NIR-2		
Value	Intercept. a_o	Slope a_1	R^2	Intercept. a_o	Slope a_1	R^2	Intercept. a_o	Slope a_1	R^2	Intercept. a_o	Slope a_1	R^2
Cairo	-0.13	1.7846	0.9496	-0.1159	1.2587	0.9325	-0.156	1.992	0.9426	-0.1254	1.3972	0.9354
Brisbane	0.1615	0.2143	0.5264	0.1745	0.2307	0.526	0.18	0.2931	0.6141	0.1423	0.3121	0.6622
Miami	0.1309	0.3374	0.7395	0.1379	0.3835	0.767	0.1373	0.4532	0.794	0.1091	0.4984	0.8304
Rio de janero	0.144	0.3584	0.7413	0.1451	0.4109	0.787	0.1448	0.4647	0.8726	0.1138	0.5402	0.8825
San Francisco	0.1316	0.37	0.8862	0.1417	0.3857	0.8266	0.1481	0.4208	0.854	0.1208	0.4341	0.8411

The intercept and slope values were applied against the slave scenes to normalize the atmospheric effects with respect to the master scene.

The next step will include applying a multi-layer classification algorithm as shown in Figure 4. More details about this algorithm can be found in[12]. This algorithm will be applied to the master scene and to the slave scenes after relative atmospheric calibration without changing the thresholds.

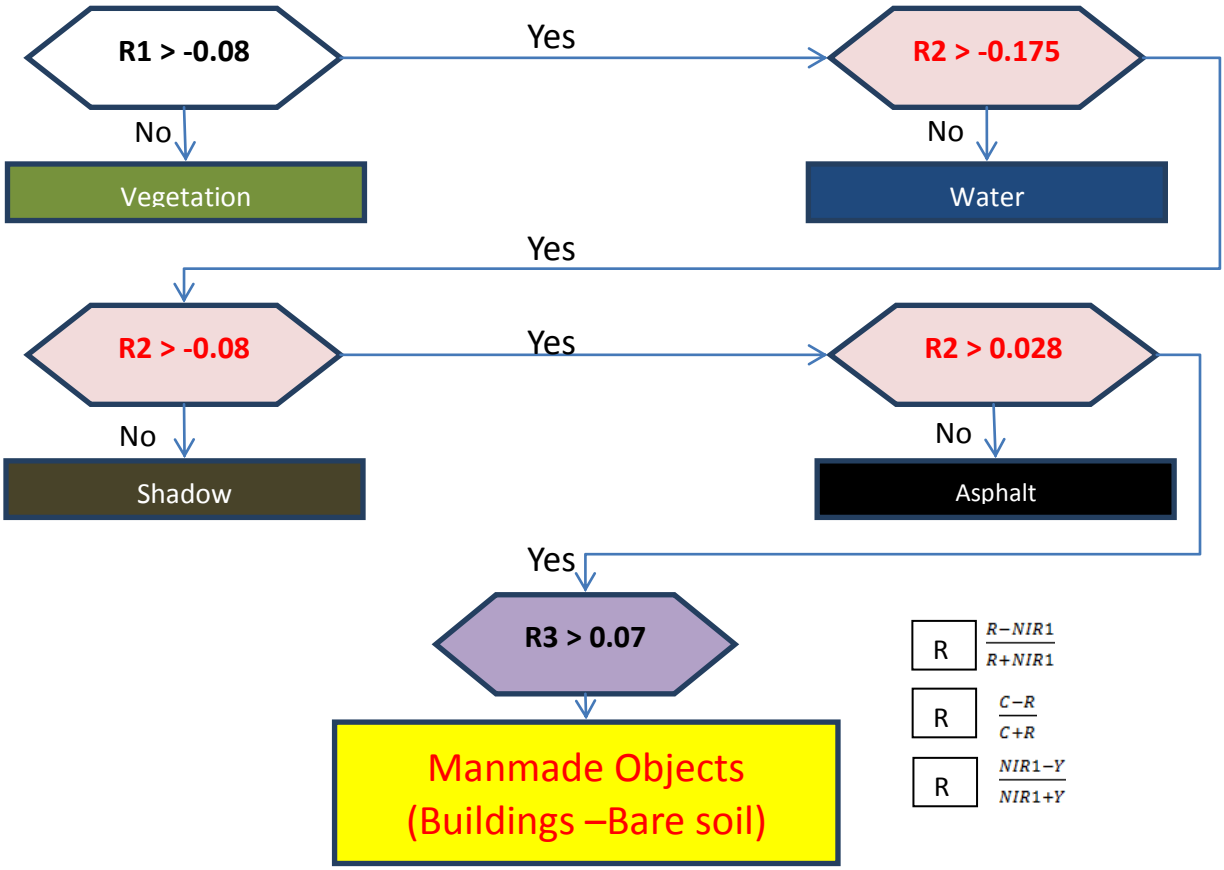

Figure 4 Applying the band ratios with the proposed thresholds[12]

III. RESULTS AND ANALYSIS

The classification results from the previous multi-layer classification step were then compared with ground truth pixels. The confusion matrices are displayed in Tables 4, 5, 6, 7 and 8.

Table 4. Confusion matrix of the slave scene "Brisbane" with ROI ground truth pixels

Overall Accuracy = 38.0273%
Kappa Coefficient = 0.3263

	Vegetation	Water	Shadow	Asphalt	Manmade	Total	Prod. Acc.	User Acc.
Vegetation	99.52	0.00	0.00	0.00	0.09	19.77	99.52	99.96
Water	0.00	0.00	0.00	0.00	0.00	0.00	0.00	0.00
Shadow	0.04	100.00	92.82	0.15	0.09	65.59	92.82	6.44
Asphalt	0.44	0.00	7.18	99.85	2.03	5.81	99.85	89.71
Manmade	0.00	0.00	0.00	0.00	97.79	8.83	97.79	100.00
Total	100.00	100.00	100.00	100.00	100.00	100.00		

Table 5. Confusion matrix of the slave scene "Cairo" with ROI ground truth pixels

Overall Accuracy = 95.5816%
Kappa Coefficient = 0.9327

	Vegetation	Water	Shadow	Asphalt	Manmade	Total	Prod. Acc.	User Acc.
Vegetation	100.00	0.00	0.00	0.00	0.00	22.81	100.00	100.00
Water	0.00	100.00	37.61	0.00	0.00	53.39	100.00	93.87

Shadow	0.00	0.00	59.33	5.07	0.00	5.46	59.33	94.63
Asphalt	0.00	0.00	3.06	86.64	0.85	5.38	86.64	93.07
Manmade	0.00	0.00	0.00	8.29	99.15	12.96	99.15	96.30
Total	100.00	100.00	100.00	100.00	100.00	100.00		

Table 6. Confusion matrix of the slave scene "Miami" with ROI ground truth pixels

Overall Accuracy = 91.2461%

Kappa Coefficient = 0.8863

	Vegetation	**Water**	**Shadow**	**Asphalt**	**Manmade**	**Total**	**Prod. Acc.**	**User Acc.**
Vegetation	100.00	0.00	0.00	0.00	0.37	13.99	100.00	99.10
Water	0.00	79.24	18.45	0.00	0.00	22.47	79.24	91.80
Shadow	0.00	20.76	81.13	0.13	0.31	13.63	81.13	59.45
Asphalt	0.00	0.00	0.42	98.85	3.11	17.32	98.85	93.71
Manmade	0.00	0.00	0.00	1.02	96.21	32.59	96.21	99.49
Total	100.00	100.00	100.00	100.00	100.00	100.00		

Table 7. Confusion matrix of the slave scene "Rio de Janero" with ROI ground truth pixels

Overall Accuracy = 97.6763%

Kappa Coefficient = 0.9630

	Vegetation	**Water**	**Shadow**	**Asphalt**	**Manmade**	**Total**	**Prod. Acc.**	**User Acc.**
Vegetation	94.58	0.00	0.00	0.00	0.00	33.80	94.58	100.00
Water	0.00	100.00	0.00	1.32	0.00	49.19	100.00	99.84
Shadow	5.39	0.00	82.73	0.66	0.00	3.07	82.74	35.82
Asphalt	0.03	0.00	16.67	97.49	0.10	6.08	97.49	96.10
Manmade	0.00	0.00	0.60	0.53	99.90	7.86	99.90	99.50
Total	100.00	100.00	100.00	100.00	100.00	100.00		

Table 8. Confusion matrix of the slave scene "San Francisco" with ROI ground truth pixels

Overall Accuracy = 98.0181%

Kappa Coefficient = 0.9725

	Vegetation	**Water**	**Shadow**	**Asphalt**	**Manmade**	**Total**	**Prod. Acc.**	**User Acc.**
Vegetation	99.61	0.00	0.28	0.00	0.59	21.97	99.61	99.61
Water	0.00	99.03	3.19	0.00	0.10	43.35	99.03	99.23
Shadow	0.04	0.97	96.15	2.07	0.29	10.52	96.15	92.75
Asphalt	0.22	0.00	0.38	95.60	3.53	14.50	95.60	97.04
Manmade	0.13	0.00	0.00	2.33	95.49	9.65	95.49	96.15
Total	100.00	100.00	100.00	100.00	100.00	100.00		

A careful study of these results showed that four out of five scenes yielded excellent producer and user accuracies for all classes when using the same classification thresholds and after applying the atmospheric normalization. Brisbane classification results were the worst since the confidence level of the linear regression was the lowest among all scenes. It was also notable that the overall accuracy and K coefficient were very high for four scenes; Cairo, Miami, Rio de Janeiro and San Francisco, compared to the Brisbane scene.

IV. CONCLUSIONS

In this study the relative atmospheric calibration process for multi-temporal WorldView-2 data was evaluated by applying a multi-layer classification algorithm with fixed thresholds against multi-temporal high resolution satellite imagery for different study areas over Brisbane, Cairo, Miami, Rio de Janeiro, San Francisco and Ismailia. The master scene was taken from the city of Ismailia. A relative atmospheric calibration process was applied to the slave scenes using manually selected PIF's. The classification algorithm was then applied to the master scene and to the slave scene after normalization. The results of this investigation show very good potentials for the use of the calibration parameters after applying the relative atmospheric normalization.

V. ACKNOWLEDGMENTS

` This work was supported in part by research funds from TECTERRA Commercialization and Research Centre, the Canada Research Chairs Program, and the Natural Science and Engineering Research Council of Canada (NSERC).
Many thanks for the ERDAS - DigitalGlobe challenge committee for providing the necessary data for this research paper.

REFERENCES

[1] J. R. Jensen, *Introductory digital image processing : a remote sensing perspective*, 3rd ed. ed.: Prentice Hall, 1994.
[2] M. El Hajj, *et al.*, "Relative Radiometric Normalization and Atmospheric Correction of a SPOT 5 Time Series," *Sensors*, vol. 8, pp. 2774-2791, 2008.
[3] T. Updike and C. Comp, "Radiometric Use of WorldView-2 Imagery," D. Globe, Ed., ed, 2010.
[4] D. Globe. (2009, the Benefits of the 8 Spectral Bands of WorldView-2. *White Paper*, 12.
[5] A. Elsharkawy, *et al.*, "A modified parallelepiped-like method for supervised classification for high resolution satellite imagery " presented at the CGU Annual Scientific Meeting, Banff, Calgary, 2011.
[6] G. Marchisio, *et al.*, "On the relative predictive value of the new spectral bands in the WorldWiew-2 sensor," in *Geoscience and Remote Sensing Symposium (IGARSS), 2010 IEEE International*, 2010, pp. 2723-2726.
[7] H. Shafri, *et al.*, "Hyperspectral Remote Sensing of Vegetation Using Red Edge Position Techniques," *American Journal of Applied Sciences*, vol. 3(6), pp. 1864-1871, 2006.
[8] M. Herold, *et al.*, "THE SPECTRAL DIMENSION IN URBAN LAND COVER MAPPING FROM HIGHRESOLUTION OPTICAL REMOTE SENSING DATA," *The 3rd Symposium on Remote Sensing of Urban Areas*, p. 8, june 2002 2002.
[9] T. Y. C. f. E. Observation. (2010). *Converting Digital Numbers to Top of Atmosphere (ToA) Reflectance*. Available: http://www.yale.edu/ceo
[10] D. Globe, "DigitalGlobe Core Imagery Products Guide," D. Globe, Ed., ed, 2009.
[11] A. Gilat and V. Subramaniam, *Numerical methods for engineers and scientists : an introduction with applications using MATLAB*. Hoboken, N.J.: Wiley, 2011.
[12] A. Elsharkawy, *et al.*, "IMPROVEMENT IN THE DETECTION OF LAND COVER CLASSES USING THE WORLDVIEW-2 IMAGERY " in *ASPRS*, Sacremento, CA, 2012, p. 11.